Density Functional Theory Calculations of Diffusion Barriers of organic Molecules through the 8-Ring of H-SSZ-13

Ashley T. Smith [a], *Philipp N. Plessow* * [a], *Felix Studt* [a,b]

[a] Institute of Catalysis Research and Technology, Karlsruhe Institute of Technology, Hermann-von-Helmholtz-Platz 1, D-76344 Eggenstein-Leopoldshafen, Germany.

[b] Institute for Chemical Technology and Polymer Chemistry, Karlsruhe Institute of Technology, Karlsruhe, 76131, Germany

Email: philipp.plessow@kit.edu

Abstract: The diffusion barriers of organic molecules through the pores of the zeolite H-SSZ-13 are investigated using periodic DFT calculations at the PBE-D3 level of theory. We calculate the diffusion barriers relative to the most stable adsorbed state on the acid site of the zeolite and find that barriers range from ~70 kJ/mol for smaller molecules such as ethene and propene up to 350 kJ/mol for durene, the largest molecule investigated here. For larger molecule, the diffusion barriers can be correlated with the vdW-radius of the diffusing molecules. For smaller molecules, which generally have smaller diffusion barriers, there is no clear correlation between the barrier and the vdW-radius. Here, the strength of adsorption at the acid site is also extremely important in determining the diffusion barrier.

Keywords: density functional theory, zeolites, diffusion, kinetics

Introduction

Zeolites are an extensively used class of materials with their main industrial applications being ion exchangers, gas separation as well as catalysis[1-3]. In catalysis, acidic zeolites are used in hydrocarbon conversion for example in fluid catalytic cracking (FCC)[4, 5] or the methanol-to-olefins process (MTO).[6-8] Here, large, sometimes branched hydrocarbons and olefins but also aromatics are formed or converted within the zeolite voids that are interconnected through pores that are typically in the one nanometer range. As a consequence, a zeolites specific activity, selectivity and stability is greatly influenced by the diffusivity of the molecules through these pores[1, 9, 10]. Addressing the diffusion limitations of molecules within zeolites is thus subject to extensive experimental [11-16] and theoretical studies.[17-38]

Theoretical studies targeting diffusion limitations are mostly focusing on smaller molecules such as e.g. propene and employ molecular dynamics simulations.[17, 19, 29] It is typically found that passing through the pores of the zeolite is an activated process resulting in a linear relationship between mean squared distance and time[17, 39]. Our aim here is to investigate larger molecules and to establish the size at which diffusion becomes prohibitive. To do this, we employ periodic density functional theory (DFT) calculations and compute the transition states for molecules passing through the pores of H-SSZ-13 exhibiting the chabazite (CHA) framework. Our focus is the diffusion process of olefins and aromatics and we specifically focus on larger molecules (e.g. benzene) in order to establish the diffusion limitations of molecules associated with the MTO process.

Results and Discussion

We model H-SSZ-13 using a unit cell with one aluminum site, with the proton located so that it is most accessible to the channel, as has been described in earlier studies[40, 41] . The cavities of this framework are connected by 8-membered rings with a geometrical diameter of 7.4 Å with respect to the position of the Si nuclei and 6.5 Å with respect to the position of the O nuclei. As depicted in Fig. 1. Effectively, the diameter experienced by diffusing molecules is smaller due repulsion between the electron shells that determine the vdW-radii of the atoms constituting the ring, resulting in a vdW-diameter of roughly 3.7 Å.

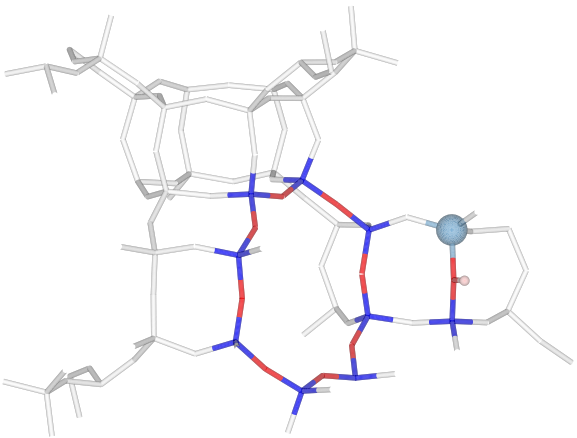

Figure 1. The structure of H-SSZ-13. The 8-membered ring and the acid site are highlighted. Silicon atoms are highlighted in blue, oxygen in red, hydrogen in pink and aluminum in light blue.

Our goal is to model diffusion of organic molecules in the limit of a low concentration of adsorbates, while the diffusion behavior at higher concentration may differ.[42] In our zeolite models, we therefore exclude coadsorption of additional molecules. Furthermore, we study a zeolite in the limit of a low acid site density. For diffusion through the eight-membered ring, we

only consider pure siliceous rings, consisting only of SiO_2-units, which is a structural motif that can be expected to occur frequently. Only a single acid site is placed within the unit cell at a position where it does not directly interfere with diffusion. The goal of including this acid site is to take into account the stabilization of adsorbates in the initial and final states before and after diffusion. This is generally expected to increase the diffusion barriers with respect to these initial and final states. We note that acid sites may also interact during diffusion, if they are located within the 8-membered ring. In agreement with a recent study[42] we have found for one such case that this leads to a stabilization of the transition state (see SI, section S7). Since purely siliceous rings are therefore expected to lead to a higher barrier, we focus on this situation for our trend study.

For adsorption at the acid site, we considered plain coordination, which leaves all chemical bonds of the adsorbate intact and results in physisorbed vdW-complexes or in some cases also π-complexes, in which the π-bond of an unsaturated organic molecule is coordinated to the acid site. To differentiate between vdW- and π-complexes, we used a simple geometric criterion, where complexes with a C-H distance smaller than 2.4 Angstrom are considered π-complexes. Plain adsorption and desorption of molecules occurs typically without energetic barrier and is simply uphill or downhill in energy. This is illustrated in Fig. 2 for the case of isobutene, where dissociation from the acid site is uphill in energy but does not require a significant barrier. Figure 2 shows, however, that there is a high a barrier for diffusion through the 8-membered ring. Additionally, we considered the formation of alkoxides, since these are also known to be stable states of olefins in zeolites. For the studied olefins, alkoxides where found to be – energetically – the most stable states only for ethylene, propylene and cyclobutene. On the other hand, MD studies indicate that π-complexes are favored over alkoxides due to entropic effects even at room temperature.[43] In contrast to plain adsorption and desorption, the formation of alkoxides requires

a distinct chemical reaction, where an O-H bond of the zeolite framework is broken and a C-H bond and a C-O bond with the olefin is formed instead. This barrier for alkoxide formation and vice versa is on the order of 120 kJ/mol for ethylene and propylene (see Table S4) and therefore much higher than the diffusion barrier. Overall, these barriers are unlikely to be a limiting factor for diffusion for two reasons. First of all, a free olefin could overcome the lower diffusion barrier many times before being trapped again as an alkoxide, which is associated with a much high barrier. Most importantly, however, in terms of free energies, alkoxides are unlikely to be the most stable species at elevated temperatures relevant for catalysis. We therefore do not consider alkoxide formation barriers in our study of diffusion barriers. Nevertheless, for consistency, we reference diffusion barriers to alkoxides, where those are the most stable states. We note that the energetic difference in stability with respect to π-complexes is at most 20 kJ/mol and alkoxides are only most stable for ethylene, propylene and cyclobutene, which have relatively low diffusion barriers so that referencing these diffusion barriers either to alkoxides or π-complexes does not make a large difference.

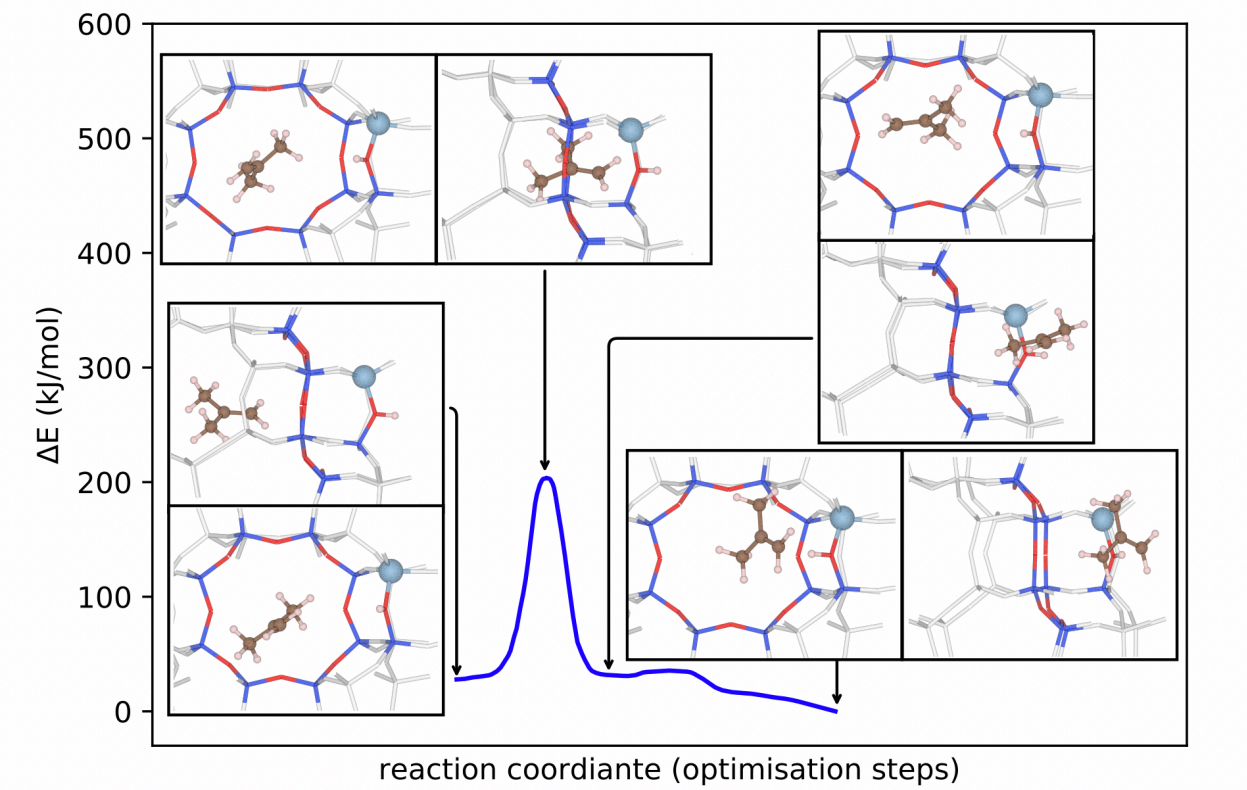

Figure 2. Energy profile for the diffusion of isobutene through the 8-membered ring. Insets illustrate the atomic structure at the indicated points of the reaction path with views both along and parallel to the ring. The energy profile was obtained by distortion of the transition state along the transition mode followed by structural optimization towards the initial and final states. Additional rearrangements of the final state that occur with low barriers were obtained with NEB-calculations.

The molecules investigated here were chosen to have incrementally increasing van der Waals diameters (d_{vdW}) with the d_{vdW} defined as the smallest cross-section that a molecule can fit inside plus an additional 2.4 Å corresponding to twice the van der Waals radius of hydrogen[44] which account for steric repulsion (see scheme 1 and Fig. 3). The minima are referenced to the most stable adsorption geometry on the acidic site within the cavity, which depending on the molecule can be a π-complex, an alkoxide or a vdW complex (see Table 1). The obtained adsorption energies are in good agreement with values from the literature.[43, 45] When the transition state is given

relative to the most stable state of the corresponding molecule it thus represents the diffusion barrier during a reaction.

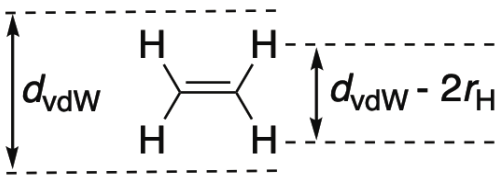

Scheme 1. Definition of d_{vdW}.

Table 1. Calculated adsorption energies and diffusion barriers for the 12 molecules investigated herein. The adsorption energies included are for the most stable adsorption configuration on the acid site of H-SSZ-13. The diffusion barriers are relative to this most stable adsorption configuration. All energies are given in kJ/mol.

Molecule	Most stable adsorbate	Adsorption energy	Diffusion barrier
Ethene	Alkoxide	-95.1	76.4
Propene	Alkoxide	-90.5	79.2
Trans-2-butene	Alkoxide	-93.0	68.9
Cyclobutene	Alkoxide	-92.2	133.1
Cis-2-butene	π-complex	-82.3	80.4
Isobutene	π-complex	-93.3	208.4
Isobutane	vdW complex	-78.8	201.0
Methanol	Hydrogen bonded	-115.3	81.5
Benzene	π-complex	-86.2	248.1

para-Xylene	vdW complex	-96.0	226.8
Tetra-methyl-ethylene	π-complex	-88.1	244.0
Durene	vdW complex	-127.1	348.5

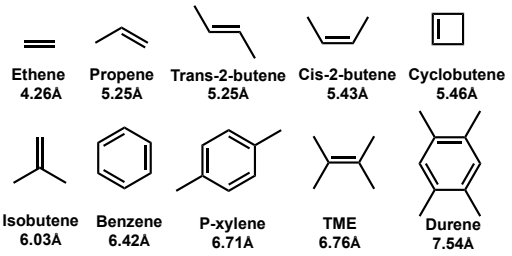

Figure 3. The d_{vdW} of ten selected molecules.

Calculations of diffusion barriers for the 12 molecules investigated here reveal three different diffusion patterns (see Fig. 4), with the shape of the energy profile and the occurrence of intermediates heavily depending upon the molecular geometry of the diffusing molecule (see Fig. 4). Isobutene exhibits one clearly distinct transition state. The diffusion of tetra-methyl-ethylene (TME) on the other hand is characterized by two symmetric transition states separated by a minimum.

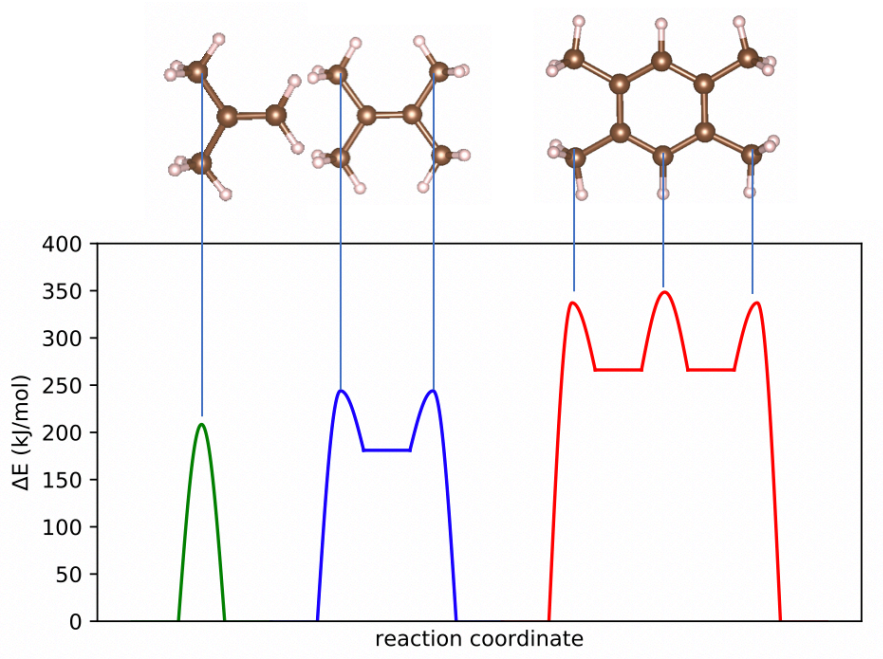

Figure 4. Schematic potential energy profile based on transition states and intermediates, for isobutene (left), tetra-methyl-ethylene (middle) and durene (right) to traverse through the 8-ring in H-SSZ-13. The adsorbed molecule at the acid site is chosen as the reference state (see also Table 1).

This can be attributed to the effective symmetry of TME. For durene, we even find three barriers which are separated by two minima, again due to the symmetry of the diffusing molecule. Importantly, we identified the transition state with the maximum barrier in all cases and will refer to these maxima as the overall diffusion barrier. Interestingly, we also find that diffusion patterns of larger molecules are accompanied by distortions of the pore structures, albeit mostly small. For durene, for example, the ring distorts and the diameter is increased by 0.73 Å (see Fig. S1 in the supplementary material for more details).

All calculated diffusion barriers are shown as a function of the d_{vdW} in Fig. 5, both with respect to the molecules in the gas-phase (Fig. 5a) and the most stable adsorption configuration (the adsorbed molecule on the acid site, Fig. 5b). As also shown in Table 1, adsorption energies for olefins and

aromatics at the acid site of H-SSZ-13 are in the range 80 – 140 kJ/mol, with the increase in vdW interactions of larger molecules being compensated by an increase in repulsion (see sections S2 and S3 of supplementary material).

The interaction of smaller olefins (ethene, propene, cis-2-butene and trans-2-butene, all with a d_{vdW} of less than 5.3 Å) with the pore is negligible, thus resulting in a constant value of around -20 kJ/mol relative to the gas-phase (Fig. 5a) (or 60-80 kJ/mol when referenced to the most stable adsorption state, Fig. 5b). These molecules will hence have relatively large diffusion constants. Olefins with d_{vdW} above 5.3 Å, on the other hand, experience strong repulsive interactions with the pore through which diffusion takes place, resulting in large diffusion barriers that increase linearly with the d_{vdW}. Isobutene (d_{vdW} = 6.03 Å) for example has a diffusion barrier of 208 kJ/mol when referenced to the most stable adsorption state. The diffusion of isobutene through the pores of H-SSZ-13 will hence be extremely slow. Diffusion of TME and benzene have even higher barriers of 244 and 248 kJ/mol, respectively. The molecule with the largest d_{vdW} (7.54 Å), durene has a diffusion barrier of 348 kJ/mol relative to the adsorbed state (Fig. 5b). Analyzing the diffusion of molecules from 5.46 Å (cyclobutene) up to a d_{vdW} of 7.54 Å (durene) we find that there is a roughly linear correlation between the magnitude of the diffusion barrier and d_{vdW}. The barriers above 5.3 Å were fitted to the function $a*d_{vdW} + b$ yielding a slope of 113 kJ/(mol*Å) with a mean absolute deviation (MAD) of 8.1 kJ/mol. Importantly, this correlation depends only on d_{vdW}. While the obtained MAD of 8.1 kJ/mol is encouraging, we note that, unfortunately, there is no clear correlation with d_{vdW} for $d_{vdW} < 6$ Å, for example when comparing the diffusion barriers of cyclobutene and cis-2-butene. It is also important to note that for these small molecules, barriers

are largely due to strong adsorption at the acid site rather than due to the barrier measured relative to the gas phase (see Fig. 5a).

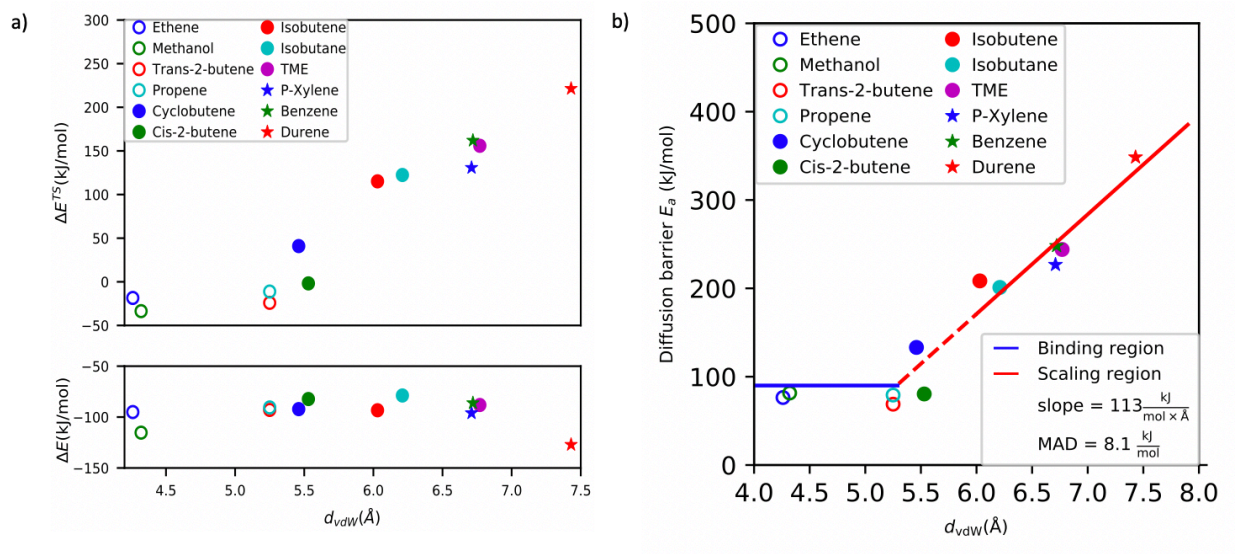

Figure 5. (a) Adsorption energies and diffusion barriers relative to the molecules in the gas-phase are shown as a function of vdW-diameter. The lower graph shows adsorption energies, the upper graph shows transition state energies. (b) Diffusion barriers as a function of vdW-diameter. The straight blue line indicates a binding region with no significant diffusion barriers. Open markers indicate molecules with a d_{vdW} below 5.3 Å. The red line indicates the scaling region with linearly increasing diffusion barriers. Filled markers indicate molecules with d_{vdW} above 5.3 Å. Circles indicate olefins and stars indicate aromatics. The red line is a linear fit with a mean absolute deviation (MAD) of 8.1 kJ/mol.

We will now turn to estimating the diffusion constants from a lattice hop model using equation 1.

$$D = \frac{l^2 k_B T}{h} e^{-\frac{E_a}{k_B T}} \quad (1)$$

Where l is the lattice parameter, k_B is the Boltzmann constant, h is the Planck constant, T is the temperature and E_a is the diffusion barrier shown in Fig. 5b. We assume a temperature of 673.15

K as this is a typical temperature for the MTO process. We also assume that the entropic contributions from the initial and transition states are similar as the diffusing molecules have nearly identical vibrational frequencies and use the computed lattice parameter of 13.6 Å for H-SSZ-13. Using these approximations and E_a = 76.4 kJ/mol as calculated for ethene we obtain a value for the diffusion constant of $3.6*10^{-11}$ m^2/s. The value is in good agreement with other theoretical studies reported in the literature (e.g. $3.8*10^{-10}$ m^2/s for ethene in SSZ-13).[17] If we take the barrier for benzene as the simplest aromatic molecule (248.1 kJ/mol) we obtain a diffusion constant of $1.4*10^{-24}$ m^2/s, indicating that diffusion of benzene is clearly limited.

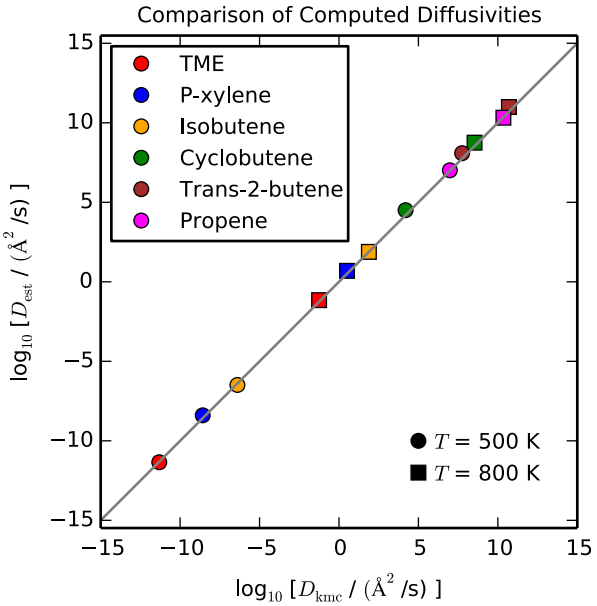

Figure 6. Comparison of diffusion constants obtained using the rate-determining step approximation as expressed in Eq. (1) with results from kMC simulations. For propene and isobutene, Eq. (1) is exact since only one minimum and transition state is included in the kMC simulation.

For the estimation of diffusion constants using Eq. (1) as discussed above, only the highest barrier relative to the most stable minimum is considered. This approximation is analogous to the rate-determining step approximation that is often applied in catalysis. As can be seen from Fig. 6, for

the range of molecules considered herein, this approximation works remarkably well, when we compare the diffusion constants obtained with Eq. (1) with diffusion constants extracted from kinetic Monte Carlo (kMC) simulations. In these kMC simulations, all elementary steps are considered and the diffusion constant is computed by analyzing the mean squared displacement obtained for 100 separate simulations with 10^5 steps each. As shown in Fig. 6, the accuracy of the diffusion constants using Eq. (1) is generally sufficient to estimate the order of magnitude of the diffusivity.

The accuracy of the diffusion constants computed in this work is mainly limited by the energies obtained with DFT and the treatment of entropic contributions. Since the main goal of this work is to determine up to which point molecules are mobile in H-SSZ-13, we expect that the accuracy is sufficient for this purpose. Most computational investigations as well as experimental studies have been focused on the diffusion of molecules with relatively high diffusion constants. For H-SSZ-13, ethylene and propylene diffusion has been investigated[17], also with respect to the effect of coadsorbates on diffusion.[42] We stress that our aim here is not to compute diffusion constants for these molecules with high accuracy. Our intention is to determine barriers in the limit where diffusion is extremely slow to determine when a molecule must be considered immobile at a given temperature. Our study is thus complementary to existing investigations, that focus on diffusion constants of more mobile molecules and compute these with high accuracy using MD-simulations and accounting for additional effects such as coadsorbates, varying acid site locations and lattice dynamics.[22, 23, 32, 42]

Conclusion

We investigated the diffusion of organic molecules through the 8 membered rings of H-SSZ-13 using DFT calculations. We considered both diffusion barriers relative to the gas phase as well as relative to the diffusing molecule being adsorbed on the acid site of H-SSZ-13. When taken relative to the adsorbed state, we calculate diffusion barriers in the range of 60-80 kJ/mol for smaller molecules, this increases for larger olefins and aromatics reaching around 200 kJ/mol for isobutene and 350 kJ/mol for durene. Furthermore, for the larger molecules, we were able to correlate the diffusion barrier with the size of the largest cross section of the molecules, denoted d_{vdW}, thus giving a simple model that enables the estimation of diffusion barriers in the limit of large molecules. However, the model does not work well for small molecules (< 5.5 Å), which have relatively low diffusion barriers. For these molecules, the strength of adsorption also becomes increasingly important in determining the height of the barrier. The established correlation is intended to give an estimate of diffusion barriers in the range where diffusion is slow to impossible, in order to predict whether or not a molecule is immobile within the zeolite.

We believe that our results shed light on the importance for the diffusion processes within zeolites for reactions where diffusion of larger olefins and aromatics plays a decisive role, e.g. as occurring in the MTO reaction or FCC. While our model has been shown to work for the chabazite framework, future work will focus on extending this to other zeolite topologies.

Methods

Periodic DFT calculations were carried out with the projector-augmented-wave (PAW) [46, 47] method using the VASP program package in version 5.3.3.4 using the standard VASP-PAWs and the Atomistic simulation environment[48]. The PBE[49, 50] functional with Grimme's dispersion corrections (PBE-D3) was used in all calculations[51]. The energy cut off was 400 eV and the

Brillouin-zone was sampled at the Γ-point with Gaussian-smearing with a width of 0.1 eV. The lengths of the vectors of the unit cells were 13.625, 13.625, and 15.067 Å as optimized in earlier studies[40] employing H-SSZ-13. The PBE-D3 functional was tested against the BEEF-vdW functional[52] that has been shown to capture the interaction of hydrocarbons with zeolites quite accurately[53] using single point calculations of the optimized structures and the same parameters as described above. Fig. S3 shows that the agreement between BEEF-vdW and PBE-D3 is quite good giving confidence to our results. In order to test whether lateral interactions with periodic images of the diffusing molecules play a significant role, we calculated the minima and the intermediate preceding the transition state for a 2 by 2 super cell for the case of benzene. Section S5 shows that the interactions are very minor such that the values for the transition state are unlikely to be affected by lateral interactions and the size of the super cell.

The dimer method[54], climbing image nudged-elastic-band[55, 56] (CI-NEB) and constrained optimizations were employed to obtain transition states. In the NEBs, Image Dependent Pair Potential (IDPP) interpolations[57] or linear interpolations were employed. Harmonic force constants were computed from a central finite difference method where only atoms in the adsorbed molecule were included. All transition states were verified to contain only a single imaginary harmonic frequency corresponding to the transition vector of the reaction. In addition, through small distortions away from the transition state followed by an optimization, a given transition states connectivity with the minima and other transition states was verified. We also tested whether including the atoms of the zeolite ring in the vibrational analysis influences the results and found that that was not the case. Finally, the transition states for the molecule to traverse the ring in both

directions were found. The good agreement is providing an extra confidence to the obtained barriers.

Competing interests

The authors declare no competing interests.

Acknowledgements

The authors acknowledge support by the state of Baden-Württemberg through bwHPC (bwunicluster and JUSTUS, RVbw17D011). Financial support from the Helmholtz Association is also gratefully acknowledged.

Associated content

The supplementary material contains a more detailed description of how the most stable state was found, data on the stretching of the ring, data comparing the PBE-D3 functional to the BEEF-vdW functional, the procedure undertaken to evaluate the size of the lateral interactions and Cartesian coordinates of optimized structures.

References

[1] S.M. Csicsery, Shape-selective catalysis in zeolites, Zeolites, 4 (1984) 202-213.
[2] N. Kosinov, J. Gascon, F. Kapteijn, E.J.M. Hensen, Recent developments in zeolite membranes for gas separation, Journal of Membrane Science, 499 (2016) 65-79.
[3] R.P. Townsend, E.N. Coker, Chapter 11 Ion exchange in zeolites, in: H. van Bekkum, E.M. Flanigen, P.A. Jacobs, J.C. Jansen (Eds.) Stud. Surf. Sci. Catal., Elsevier, 2001, pp. 467-524.
[4] A. Primo, H. Garcia, Zeolites as catalysts in oil refining, Chem. Soc. Rev., 43 (2014) 7548-7561.
[5] E.T.C. Vogt, B.M. Weckhuysen, Fluid catalytic cracking: recent developments on the grand old lady of zeolite catalysis, Chem. Soc. Rev., 44 (2015) 7342-7370.

[6] U. Olsbye, S. Svelle, M. Bjørgen, P. Beato, T.V. Janssens, F. Joensen, S. Bordiga, K.P. Lillerud, Conversion of methanol to hydrocarbons: how zeolite cavity and pore size controls product selectivity, Angew. Chem. Int. Ed., 51 (2012) 5810-5831.
[7] U. Olsbye, S. Svelle, K.P. Lillerud, Z.H. Wei, Y.Y. Chen, J.F. Li, J.G. Wang, W.B. Fan, The formation and degradation of active species during methanol conversion over protonated zeotype catalysts, Chem. Soc. Rev., 44 (2015) 7155-7176.
[8] M. Stöcker, Methanol-to-hydrocarbons: catalytic materials and their behavior, Microporous Mesoporous Mater., 29 (1999) 3-48.
[9] B. Smit, T.L.M. Maesen, Towards a molecular understanding of shape selectivity, Nature, 451 (2008) 671-678.
[10] B.P.C. Hereijgers, F. Bleken, M.H. Nilsen, S. Svelle, K.-P. Lillerud, M. Bjørgen, B.M. Weckhuysen, U. Olsbye, Product shape selectivity dominates the Methanol-to-Olefins (MTO) reaction over H-SAPO-34 catalysts, J. Catal., 264 (2009) 77-87.
[11] S.J. Reitmeier, R.R. Mukti, A. Jentys, J.A. Lercher, Surface Transport Processes and Sticking Probability of Aromatic Molecules in HZSM-5, J. Phys. Chem. C, 112 (2008) 2538-2544.
[12] S.R. Zheng, H. Tanaka, A. Jentys, J.A. Lercher, Novel model explaining toluene diffusion in HZSM-5 after surface modification, J. Phys. Chem. B, 108 (2004) 1337-1343.
[13] G. Muller, T. Narbeshuber, G. Mirth, J.A. Lercher, Infrared Microscopic Study of Sorption and Diffusion of Toluene in Zsm-5, J. Phys. Chem., 98 (1994) 7436-7439.
[14] P. Losch, A.B. Pinar, M.G. Willinger, K. Soukup, S. Chavan, B. Vincent, P. Pale, B. Louis, H-ZSM-5 zeolite model crystals: Structure-diffusion-activity relationship in methanol-to-olefins catalysis, J. Catal., 345 (2017) 11-23.
[15] R. Kolvenbach, N. Al-Yassir, S.S. Al-Khattaf, O.C. Gobin, J.H. Ahn, A. Jentys, J.A. Lercher, A comparative study of diffusion of benzene/p-xylene mixtures in MFI particles, pellets and grown membranes, Catal. Today, 168 (2011) 147-157.
[16] O.C. Gobin, S.J. Reitmeier, A. Jentys, J.A. Lercher, Diffusion pathways of benzene, toluene and p-xylene in MFI, Microporous Mesoporous Mater., 125 (2009) 3-10.
[17] A. Ghysels, S.L.C. Moors, K. Hemelsoet, K. De Wispelaere, M. Waroquier, G. Sastre, V. Van Speybroeck, Shape-Selective Diffusion of Olefins in 8-Ring Solid Acid Microporous Zeolites, J. Phys. Chem. C, 119 (2015) 23721-23734.
[18] B. Smit, T.L.M. Maesen, Molecular Simulations of Zeolites: Adsorption, Diffusion, and Shape Selectivity, Chem. Rev., 108 (2008) 4125-4184.
[19] R.V. Awati, P.I. Ravikovitch, D.S. Sholl, Efficient and Accurate Methods for Characterizing Effects of Framework Flexibility on Molecular Diffusion in Zeolites: CH4 Diffusion in Eight Member Ring Zeolites, J. Phys. Chem. C, 117 (2013) 13462-13473.
[20] J.M. Lin, C.T. He, P.Q. Liao, R.B. Lin, J.P. Zhang, Structural, energetic, and dynamic insights into the abnormal xylene separation behavior of hierarchical porous crystal, Sci Rep, 5 (2015) 11537.
[21] D.C. Ford, D. Dubbeldam, R.Q. Snurr, V. Kunzel, M. Wehring, F. Stallmach, J. Karger, U. Muller, Self-Diffusion of Chain Molecules in the Metal-Organic Framework IRMOF-1: Simulation and Experiment, J. Phys. Chem. Lett., 3 (2012) 930-933.
[22] J. Liu, S. Keskin, D.S. Sholl, J.K. Johnson, Molecular Simulations and Theoretical Predictions for Adsorption and Diffusion of CH4/H2 and CO2/CH4 Mixtures in ZIFs, The Journal of Physical Chemistry C, 115 (2011) 12560-12566.

[23] E. Haldoupis, S. Nair, D.S. Sholl, Efficient calculation of diffusion limitations in metal organic framework materials: a tool for identifying materials for kinetic separations, J. Am. Chem. Soc., 132 (2010) 7528-7539.
[24] R. Xiong, J.T. Fern, D.J. Keffer, M. Fuentes-Cabrera, D.M. Nicholson, Molecular simulations of adsorption and diffusion of RDX in IRMOF-1, Mol. Simulat., 35 (2009) 910-919.
[25] S. Keskin, J. Liu, J.K. Johnson, D.S. Sholl, Atomically detailed models of gas mixture diffusion through CuBTC membranes, Microporous Mesoporous Mater., 125 (2009) 101-106.
[26] R. Babarao, Y.H. Tong, J.W. Jiang, Molecular Insight into Adsorption and Diffusion of Alkane Isomer Mixtures in Metal-Organic Frameworks, J. Phys. Chem. B, 113 (2009) 9129-9136.
[27] R. Babarao, J.W. Jiang, Unraveling the Energetics and Dynamics of Ibuprofen in Mesoporous Metal-Organic Frameworks, J. Phys. Chem. C, 113 (2009) 18287-18291.
[28] S. Amirjalayer, R. Schmid, Mechanism of benzene diffusion in MOF-5: A molecular dynamics investigation, Microporous Mesoporous Mater., 125 (2009) 90-96.
[29] B. Smit, T.L. Maesen, Molecular simulations of zeolites: adsorption, diffusion, and shape selectivity, Chem. Rev., 108 (2008) 4125-4184.
[30] B. Liu, E. Garcia-Perez, D. Dubbeldam, B. Smit, S. Calero, Understanding Aluminum Location and Non-framework Ions Effects on Alkane Adsorption in Aluminosilicates: A Molecular Simulation Study, J. Phys. Chem. C, 111 (2007) 10419-10426.
[31] E. Garcia-Perez, D. Dubbeldam, B. Liu, B. Smit, S. Calero, A computational method to characterize framework aluminum in aluminosilicates, Angew. Chem. Int. Ed. Engl., 46 (2007) 276-278.
[32] S. Amirjalayer, M. Tafipolsky, R. Schmid, Molecular Dynamics Simulation of Benzene Diffusion in MOF-5: Importance of Lattice Dynamics, Angew. Chem. Int. Ed., 46 (2007) 463-466.
[33] D.S. Sholl, Understanding macroscopic diffusion of adsorbed molecules in crystalline nanoporous materials via atomistic simulations, Acc. Chem. Res., 39 (2006) 403-411.
[34] A.I. Skoulidas, D.S. Sholl, Molecular dynamics Simulations of self-diffusivities, corrected diffusivities, and transport diffusivities of light gases in four silica zeolites to assess influences of pore shape and connectivity, J. Phys. Chem. A, 107 (2003) 10132-10141.
[35] A.I. Skoulidas, D.S. Sholl, Direct tests of the Darken approximation for molecular diffusion in zeolites using equilibrium molecular dynamics, J. Phys. Chem. B, 105 (2001) 3151-3154.
[36] D.S. Sholl, R.T. Skodje, Diffusion of clusters of atoms and vacancies on surfaces and the dynamics of diffusion-driven coarsening, Phys. Rev. Lett., 75 (1995) 3158-3161.
[37] G. Sastre, C.R.A. Catlow, A. Corma, Diffusion of benzene and propylene in MCM-22 zeolite. A molecular dynamics study, J. Phys. Chem. B, 103 (1999) 5187-5196.
[38] G. Sastre, N. Raj, C.R.A. Catlow, R. Roque-Malherbe, A. Corma, Selective diffusion of C8 aromatics in a 10 and 12 MR zeolite. A molecular dynamics study, J. Phys. Chem. B, 102 (1998) 3198-3209.
[39] D. Dubbeldam, E. Beerdsen, S. Calero, B. Smit, Dynamically corrected transition state theory calculations of self-diffusion in anisotropic nanoporous materials, J. Phys. Chem. B, 110 (2006) 3164-3172.
[40] P.N. Plessow, F. Studt, Unraveling the Mechanism of the Initiation Reaction of the Methanol to Olefins Process Using ab Initio and DFT Calculations, ACS Catal., 7 (2017) 7987-7994.

[41] P.N. Plessow, F. Studt, Theoretical Insights into the Effect of the Framework on the Initiation Mechanism of the MTO Process, Catal. Lett., 148 (2018) 1246-1253.
[42] P. Cnudde, R. Demuynck, S. Vandenbrande, M. Waroquier, G. Sastre, V.V. Speybroeck, Light Olefin Diffusion during the MTO Process on H-SAPO-34: A Complex Interplay of Molecular Factors, J. Am. Chem. Soc., 142 (2020) 6007-6017.
[43] P. Cnudde, K. De Wispelaere, J. Van der Mynsbrugge, M. Waroquier, V. Van Speybroeck, Effect of temperature and branching on the nature and stability of alkene cracking intermediates in H-ZSM-5, J. Catal., 345 (2017) 53-69.
[44] R.S. Rowland, R. Taylor, Intermolecular nonbonded contact distances in organic crystal structures: Comparison with distances expected from van der Waals radii, J. Phys. Chem., 100 (1996) 7384-7391.
[45] P.N. Plessow, F. Studt, Olefin methylation and cracking reactions in H-SSZ-13 investigated with ab initio and DFT calculations, Catal. Sci. Technol., 8 (2018) 4420-4429.
[46] G. Kresse, D. Joubert, From Ultrasoft Pseudopotentials to the Projector Augmented-Wave Method, Phys. Rev. B, 59 (1999) 1758-1775.
[47] G. Kresse, J. Furthmuller, Efficient Iterative Schemes for Ab Initio Total-Energy Calculations using a Plane-Wave Basis Set, Phys. Rev. B, 54 (1996) 11169-11186.
[48] A. Hjorth Larsen, J. Jørgen Mortensen, J. Blomqvist, I.E. Castelli, R. Christensen, M. Dułak, J. Friis, M.N. Groves, B. Hammer, C. Hargus, E.D. Hermes, P.C. Jennings, P. Bjerre Jensen, J. Kermode, J.R. Kitchin, E. Leonhard Kolsbjerg, J. Kubal, K. Kaasbjerg, S. Lysgaard, J. Bergmann Maronsson, T. Maxson, T. Olsen, L. Pastewka, A. Peterson, C. Rostgaard, J. Schiøtz, O. Schütt, M. Strange, K.S. Thygesen, T. Vegge, L. Vilhelmsen, M. Walter, Z. Zeng, K.W. Jacobsen, The atomic simulation environment—a Python library for working with atoms, J. Phys.: Condens. Matter, 29 (2017) 273002.
[49] J.P. Perdew, K. Burke, M. Ernzerhof, Generalized Gradient Approximation Made Simple Phys. Rev. Lett., 78 (1997) 1396-1396.
[50] J.P. Perdew, A. Ruzsinszky, G.I. Csonka, O.A. Vydrov, G.E. Scuseria, L.A. Constantin, X. Zhou, K. Burke, Erratum: Restoring the Density-Gradient Expansion for Exchange in Solids and Surfaces [Phys. Rev. Lett.100, 136406 (2008)], Phys. Rev. Lett., 102 (2009) 039902.
[51] S. Grimme, J. Antony, S. Ehrlich, H. Krieg, A consistent and accurate ab initio parametrization of density functional dispersion correction (DFT-D) for the 94 elements H-Pu, J. Chem. Phys., 132 (2010).
[52] J. Wellendorff, K.T. Lundgaard, A. Mogelhoj, V. Petzold, D.D. Landis, J.K. Nørskov, T. Bligaard, K.W. Jacobsen, Density functionals for surface science: Exchange-correlation model development with Bayesian error estimation, Phys. Rev. B, 85 (2012) 235149.
[53] R.Y. Brogaard, P.G. Moses, J.K. Nørskov, Modeling van der Waals Interactions in Zeolites with Periodic DFT: Physisorption of n-Alkanes in ZSM-22, Catal. Lett., 142 (2012) 1057-1060.
[54] G. Henkelman, H. Jonsson, A dimer method for finding saddle points on high dimensional potential surfaces using only first derivatives, J. Chem. Phys., 111 (1999) 7010-7022.
[55] G. Henkelman, H. Jónsson, Improved tangent estimate in the nudged elastic band method for finding minimum energy paths and saddle points, J. Chem. Phys., 113 (2000) 9978-9985.
[56] G. Henkelman, B.P. Uberuaga, H. Jónsson, A climbing image nudged elastic band method for finding saddle points and minimum energy paths, J. Chem. Phys., 113 (2000) 9901-9904.
[57] S. Smidstrup, A. Pedersen, K. Stokbro, H. Jonsson, Improved initial guess for minimum energy path calculations, J. Chem. Phys., 140 (2014) 214106.